01 Apr 2008

Synthesis and Characterization of Two Metallic Spin-Glass Phases of $FeMo_4Ge_3$

Peter J. Baker

Peter D. Battle

Stephen J. Blundell

Fernande Grandjean
Missouri University of Science and Technology, grandjeanf@mst.edu

et. al. For a complete list of authors, see https://scholarsmine.mst.edu/chem_facwork/2428

Synthesis and characterization of two metallic spin-glass phases of $FeMo_4Ge_3$

Peter J. Baker,[1] Peter D. Battle,[2,*,†] Stephen J. Blundell,[1,*,‡] Fernande Grandjean,[3] Tom Lancaster,[1] Gary J. Long,[4] Sophie E. Oldham,[2] and Timothy J. Prior[2]

[1]*Clarendon Laboratory, Oxford University, Parks Road, Oxford OX1 3PU, United Kingdom*

[2]*Inorganic Chemistry Laboratory, Oxford University, South Parks Road, Oxford OX1 3QR, United Kingdom*

[3]*Department of Physics, University of Liège, B5, B-4000 Sart-Tilman, Belgium*

[4]*Department of Chemistry, University of Missouri-Rolla, Rolla, Missouri 65409-0010, USA*

(Received 19 April 2007; revised manuscript received 9 November 2007; published 2 April 2008)

Polycrystalline samples of $FeMo_4Ge_3$ have been synthesized by the reduction of an oxide mixture at 1248 K and characterized by a combination of diffraction, muon spin relaxation (μ^+SR), Mössbauer spectroscopy, magnetometry, transport, and heat-capacity measurements. The compound adopts a tetragonal W_5Si_3 structure (space group $I4/mcm$); the iron and molybdenum atoms are disordered over two crystallographic sites, 16*k* and either 4*a* or 4*b*. The synthesis conditions determine which fourfold site is selected; occupation of either leads to the presence of one-dimensional chains of transition metals in the structure. In both cases, the electrical resistivity below 200 K is ~175 $\mu\Omega$ cm. The dc magnetization rapidly rises below 35 K (Fe/Mo on 16*k* and 4*b* sites) or 16 K (16*k* and 4*a* sites), and a magnetization of $1\mu_B$ or $0.8\mu_B$ per Fe atom is observed in 4 T at 2 K. The ac susceptibility and the heat capacity both suggest that these are glasslike magnetic transitions, although the transition shows a more complex temperature dependence (with two maxima in χ'') when the 4*b* sites are partially occupied by iron. No long-range magnetic order is thought to be present at 5 K in either structural form; this has been proven by neutron diffraction and μ^+SR for the case when Fe and Mo occupy the 16*k* and 4*b* sites.

DOI: 10.1103/PhysRevB.77.134405 PACS number(s): 71.20.Lp, 75.50.Lk, 76.75.+i

INTRODUCTION

The interplay between theoretical and experimental solid-state physics relies to some extent on the availability of compounds that can be used to exemplify the relatively simple permutations of structure and properties that can be modeled using the methods currently available. Unfortunately, chemistry is not always able to provide a suitable material, although there are occasions when a compound synthesized in an attempt to exemplify a selected permutation fails to satisfy the specified criteria, yet shows interesting behavior in its own right. We describe such a compound below.

The details of what has become known as the W_5Si_3 structure were first elucidated by Aronsson.[1] There are four formula units in the tetragonal unit cell (space group $I4/mcm$), with the nonmetal atoms occupying the 4*a* site and an 8*h* site, and the transition-metal atoms occupying the 4*b* site and a 16*k* site. The crystal structure is illustrated in Fig. 1. It can be seen [Fig. 1(a)] that the atoms on both of the fourfold sites form chains parallel to [001] with an interatomic distance of 0.5*c* (~2.45 Å) along the chains. Each 4*b* transition-metal atom [Fig. 1(b)] also has four 8*h* nonmetal neighbors at a distance of ~2.65 Å, and eight 16*k* transition-metal atoms in a coordination shell of radius ~3.05 Å. The nonmetals and metals lie at the vertices of distorted tetrahedra and square antiprisms, respectively. The chain-forming nonmetal atoms also have eight equidistant (~2.65 Å) 16*k* transition-metal neighbors at the vertices of a square antiprism [Fig. 1(c)]. The remaining transition-metal atoms, those on the 16*k* sites, are surrounded by six nonmetal atoms, three other 16*k* transition-metal atoms at a distance of ~2.75 Å, and two 4*b* transition metals at a distance of ~3.05 Å.

Other compositions that have been shown to adopt this structure include Mo_5Si_3 (Ref. 1) and Mo_5Ge_3.[2–5] $Zr_5M_{1-x}Pn_{2+x}$ (M=Cr and Mn; Pn=Sb and Bi) is a more complex, metal-rich example,[6] in which the 4*a* site is partially occupied by an element from the first row of the *d* block; Pauli paramagnetism and Curie–Weiss ($\theta<0$) behavior have been observed for M=Cr and Mn, respectively. In this paper, we describe the synthesis and characterization of $FeMo_4Ge_3$. This composition, with a 1:4 Fe:Mo ratio, was chosen for study because atomic ordering of Fe and Mo over the 4*b* and 16*k* sites, respectively, would produce a structure containing isolated linear chains of iron atoms (Fig. 1) in a diamagnetic matrix, which could therefore serve as a model for the study of one-dimensional magnetic behavior; the shortest interchain Fe-Fe distance would be ~6.8 Å. In fact, this ordering does not occur. The iron atoms partially occupy the 16*k* site and, depending on the synthesis conditions, either the 4*a* or the 4*b* site. We shall show below that when the iron occupies the 4*a* site and the 16*k* site, a magnetic behavior resembling that of a magnetically dilute spin glass is observed. However, the presence of iron on both the 16*k* site and the 4*b* site leads to more complex spin-glass behavior, which markedly contrasts that observed in canonical spin glasses, be they insulating or metallic.[7–9] The observed behavior also contrasts that of the one-dimensional compounds YMn_4Al_8 and $LaMn_4Al_8$ where, in the absence of structural disorder, a pseudogap was observed in the spin-excitation spectrum.[10,11]

EXPERIMENT

Polycrystalline samples of $FeMo_4Ge_3$ were synthesized by heating stoichiometric mixtures of high-purity (Alfa Ae-

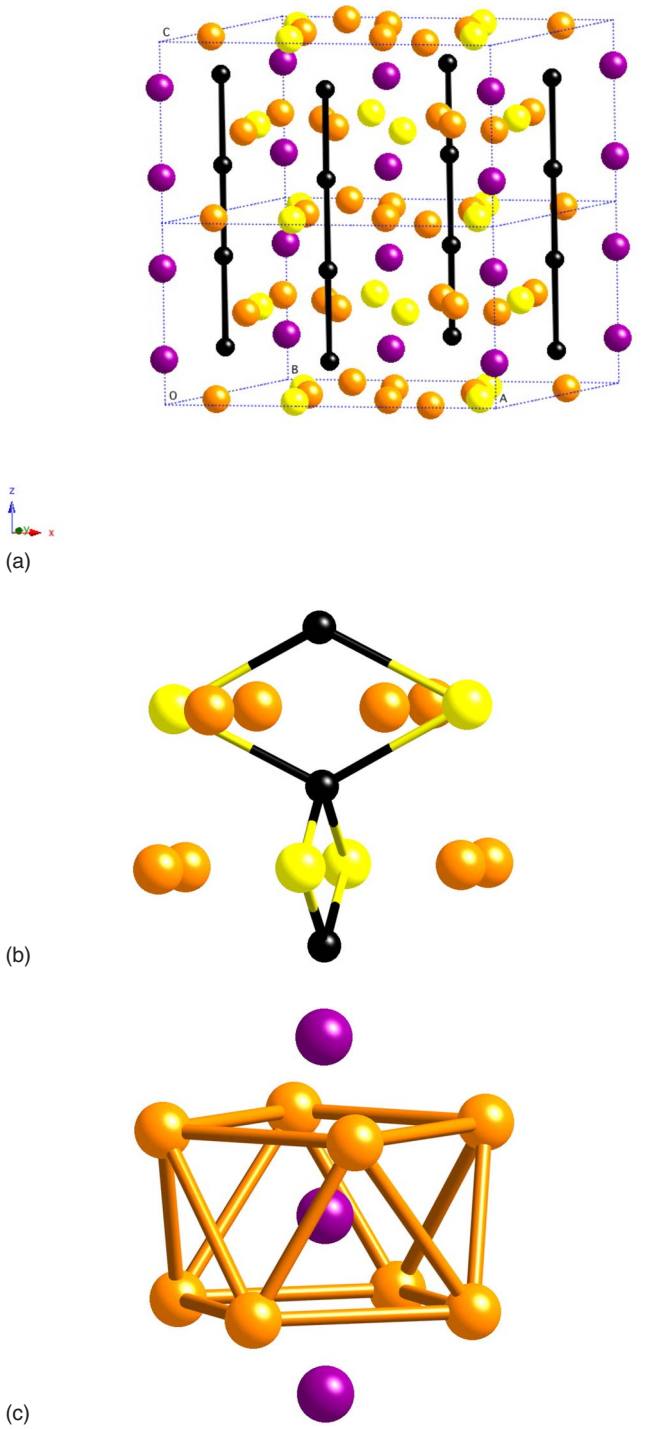

FIG. 1. (Color online) W_5Si_3 structure type: light (yellow), dark (purple), and medium (orange) shaded large circles represent Si (8*h*), Si (4*a*), and W (16*k*) atoms, respectively. Small black circles represent W (4*b*) atoms in (a) the unit cell; black lines are drawn to emphasize the chains of 4*b*-site atoms parallel to [001]. (b) The environment of the 4*b* site, showing tetrahedral coordination by 8*h* sites. (c) The environment of the 4*a* site.

sar, ≥99.998%) Fe_2O_3, MoO_3, and GeO_2 under a flow of 10% dihydrogen in argon at a nominal temperature of 973 K for 48 h, followed by 24 h at 1023 and 1148 K, and 120 h at 1248 K. The product was cooled in the gas flow. The x-ray diffraction patterns of the final products (samples A and B) were recorded at room temperature on a Siemens D5000 diffractometer using Cu $K\alpha_1$ radiation. Neutron diffraction data were subsequently collected on sample A at room temperature and 5 K over the angular range $5° \leqslant 2\theta \leqslant 150°$ using the diffractometer D2b at ILL Grenoble; a mean neutron wavelength $\lambda = 1.594$ Å was selected. All diffraction data were analyzed using the Rietveld[12] method, as implemented in the GSAS program package.[13] A Quantum Design Physical Property Measurement System (PPMS) was used to measure the temperature dependence of the ac electrical resistivity of both samples using a five-point Hall-effect geometry in a 10 mT magnetic field. The measurements were repeated in fields of 5 and 10 T for sample A. Zero-field muon-spin relaxation (μ^+SR) measurements were made on a powder of sample A using the GPS instrument at the Paul Scherrer Institute, Switzerland, using a ^{4}He cryostat. The sample was wrapped in silver foil and mounted on a silver sample holder. In a μ^+SR experiment,[14] spin-polarized positive muons are stopped in a target sample, where the muon usually occupies an interstitial position in the crystal. The observed property in the experiment is the time evolution of the muon-spin polarization, the behavior of which depends on the local magnetic field at the muon site. Each muon decays, with a lifetime of 2.2 μs, into two neutrinos and a positron, the latter particle being emitted preferentially along the instantaneous direction of the muon spin. Recording the time dependence of the positron emission directions therefore allows the determination of the spin polarization of the ensemble of muons. In our experiments, the emission of positrons from the muons implanted in our sample is recorded by forward (F) and backward (B) counters as a function of time and stored in the histograms $N_F(t)$ and $N_B(t)$, respectively. The quantity of interest is the decay positron asymmetry function defined by

$$A(t) = [N_F(t) - \alpha N_B(t)]/[N_F(t) + \alpha N_B(t)],$$

where α is an experimental calibration constant close to unity. $A(t)$ is thus proportional to the spin polarization of the muon ensemble.

The heat capacity of sintered pellets of samples A and B was measured by a 2τ relaxation method[15] using a Quantum Design PPMS. The temperature dependence of the dc magnetic susceptibility was determined in an applied field of

TABLE I. Structural parameters of $FeMo_4Ge_3$ (sample A) at room temperature. [Space group $I4/mcm$; $a = 9.779\,13(9)$ Å, $c = 4.893\,41(5)$ Å; $\chi^2 = 4.4$; $R_{wpr} = 3.9\%$.]

Atom	(site)	*x*	*y*	*z*	U_{iso} (Å^2)
Mo/Fe	(16*k*)[a]	0.07813(9)	0.22747(8)	0	0.0089(2)
Mo/Fe	(4*b*)[b]	0	1/2	1/4	0.0102(4)
Ge1	(8*h*)	0.16250(7)	0.66250(7)	0	0.0091(2)
Ge2	(4*a*)	0	0	1/4	0.0063(3)

[a]Site occupancy Mo:Fe 92.9(4)%:7.1(4)%
[b]Site occupancy Mo:Fe 28(2)%:72(2)%

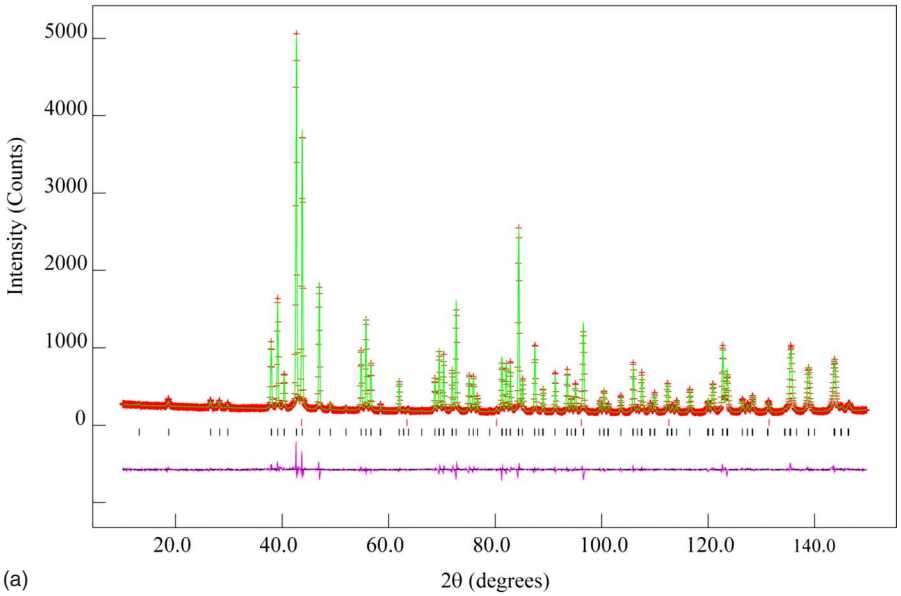

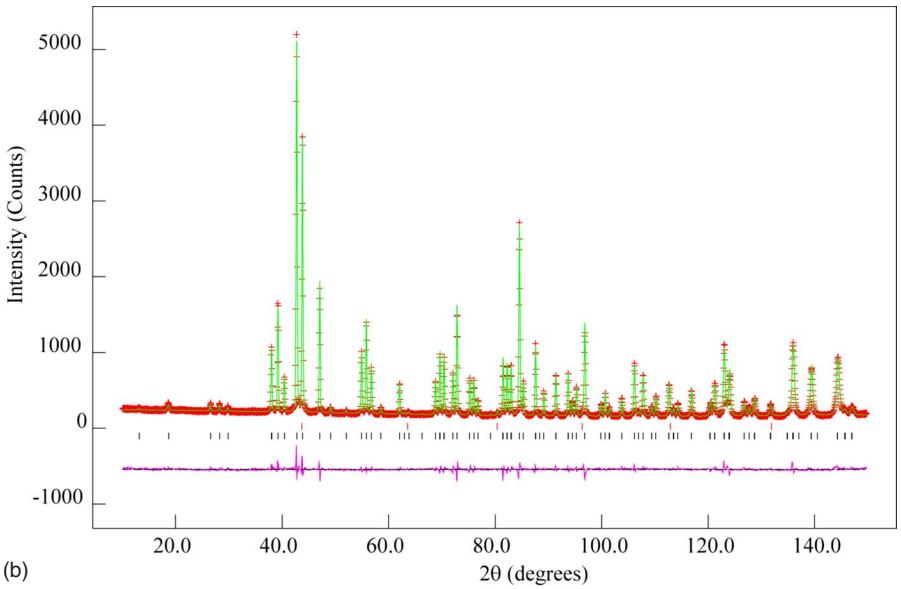

FIG. 2. (Color online) Observed (+, red) and calculated (−, green) neutron diffraction profiles of $FeMo_4Ge_3$ (sample A) at (a) room temperature and (b) 5 K. Difference curves (−, purple) are plotted below. Upper and lower reflection markers are related to the vanadium sample container and the sample, respectively.

10 mT using a Quantum Design MPMS superconducting quantum interference device (SQUID) magnetometer. Each sample, in powder form, was heated from 2 to 300 K after cooling in both zero applied field [zero-field cooled (ZFC)] and in the measuring field [field cooled (FC)]. The field dependence of the sample magnetization was also determined at selected temperatures and, in the case of sample A, the thermal-remanent magnetization was measured after cooling the sample to 2 K in a field of 0.1 T. A drive field of 0.1 mT was used to measure the ac susceptibility as a function of frequency ($0.5\ \text{Hz} \leqslant \omega \leqslant 10^3$ Hz) over the temperature range $2\ \text{K} \leqslant T \leqslant 40$ K in a dc field of <0.1 mT. In the case of sample A, measurements of the ac susceptibility were also made in small applied dc fields to investigate whether the applied field has any effect on the transitions seen in the zero-field ac susceptibility measurements and in the heat capacity.

The iron-57 Mössbauer spectra of samples A and B have been measured as a function of temperature ($4.2\ \text{K} \leqslant T \leqslant 295$ K) on a constant acceleration spectrometer that utilized a rhodium matrix cobalt-57 source and was calibrated at 295 K with α-iron foil. The isomer shifts are reported relative to α-iron at 295 K. The absorber thickness was 40 mg/cm^2.

RESULTS

Our study of $FeMo_4Ge_3$ originally involved only sample A. However, the characterization of a material produced in a later synthesis (sample B) revealed inconsistent behavior. Further investigation showed that this was attributable to the presence of two variants of $FeMo_4Ge_3$, which are produced by marginally different synthesis procedures. The data recorded on each variant were self-consistent. We describe below the behavior of both forms of $FeMo_4Ge_3$, but as a consequence of the history recounted above, sample A has been studied in somewhat more depth than sample B, for example, by neutron diffraction and μ^+SR.

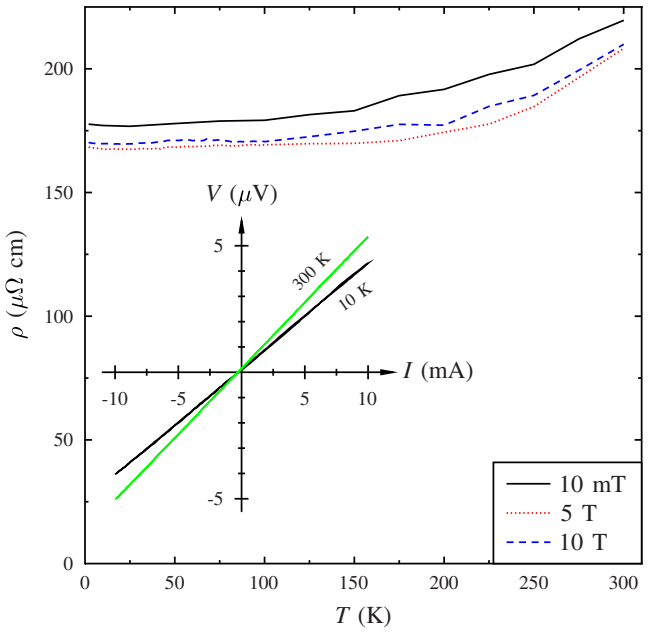

FIG. 3. (Color online) Resistivity of $FeMo_4Ge_3$ (sample A) as a function of temperature measured in three magnetic fields using a five-contact measurement, which permitted the extraction of both resistivity (shown) and Hall coefficient (not shown) as described in the text. (Inset) $V(I)$ curves at 10 and 300 K, showing Ohmic behavior.

All of the peaks in the x-ray diffraction pattern of each reaction product could be indexed in space group $I4/mcm$, which is consistent with the adoption of the W_5Si_3 structure. Similarly, no impurity phases were apparent in the neutron diffraction data collected at room temperature, although Bragg peaks from the vanadium sample container were observed. It became clear during the analysis of the data sets collected from sample A that the Fe and Mo atoms were partially disordered over the 4*b* and 16*k* sites. The structural parameters derived from neutron diffraction data are summarized in Table I and the fitted diffraction pattern is shown in Fig. 2(a). The model devised to account for the Bragg scattering at room temperature was also able to account for the scattering observed at 5 K, as shown by Fig. 2(b). This model was also able to account (R_{wpr}=5.15%) for the room-temperature x-ray diffraction pattern of sample B, although the unit-cell parameters [a=9.7856(1) Å and c =4.883 97(5) Å] were somewhat different from those of sample A, and the atomic distribution on the 4*b* site was refined to be 58.5(9)% Fe and 41.5% Mo. We shall return to this point below.

The electrical resistivity of type-A $FeMo_4Ge_3$ is largely independent of temperature and applied magnetic field below 250 K (Fig. 3) and remains Ohmic throughout the measured temperature range (Fig. 3 inset). The magnitude of the resistivity $\rho \sim 175$ $\mu\Omega$ cm leads us to regard this compound as a bad metal. The Hall coefficient (R_H) is positive at all measured temperatures (5 K$<T<$300 K), suggesting that holes dominate the electrical conductivity. The magnitude of R_H remains approximately constant across this temperature range, and shows no anomaly close to the magnetic transition, demonstrating that R_H is dominated by the ordinary, rather than the anomalous, Hall coefficient. From the value of the Hall coefficient, we estimate the net carrier concentration $n(=1/eR_H)$ to be close to 2×10^{19} cm^{-3}. Assuming $m^* \sim m_e$, the measured resistivity and carrier concentration lead to an estimate of the scattering time $\tau=(m^*/ne^2\rho)\sim10^{-12}$ s and carrier free path $\lambda=v_F\tau\sim1$ nm, justifying the description of $FeMo_4Ge_3$ as a bad metal. There appears to be a small negative magnetoresistance in a field of 5 T, but little further change in resistivity is observed in fields above 5 T. The resistivity of sample B is essentially temperature independent and takes the value of 175 $\mu\Omega$ cm, very similar to that found for sample A.

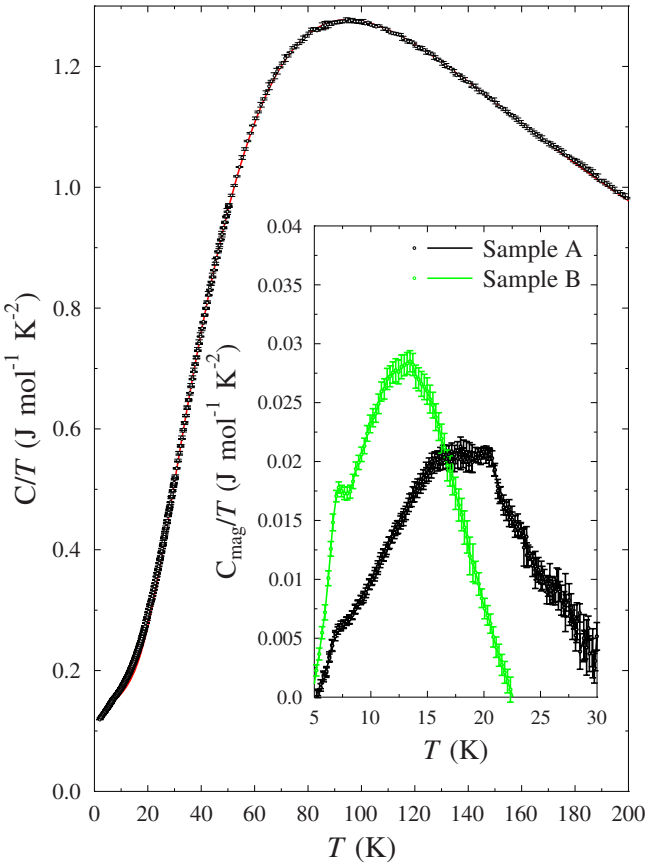

FIG. 4. (Color online) Heat-capacity data for $FeMo_4Ge_3$ (sample A) with a line showing the fit described in the text. The inset shows the region around the magnetic transitions for both samples A and B, with the fitted lattice and electronic heat capacity subtracted from the data. The line is a guide for the eye.

The heat capacity of sample A at temperatures below 200 K is shown in Fig. 4. The data are dominated by the lattice and electronic components. The former were modeled using a Debye mode and an Einstein mode, and the latter by a term linear in temperature. This resulted in the solid line shown in Fig. 4, which describes the data reasonably well. The fitted parameters are the Debye temperature, Θ_D=380(8) K, the Einstein temperature, Θ_E=157(3) K, and, for the electronic component, γ=0.144 J mol^{-1} K^{-2}. We note that a crude estimate of γ using a value of $E_F \sim 26$ meV (obtained from the Hall effect data assuming $m^* \sim m_e$ andthe free electron model) yields $\gamma=\pi^2k_B^2N_A/2E_F$

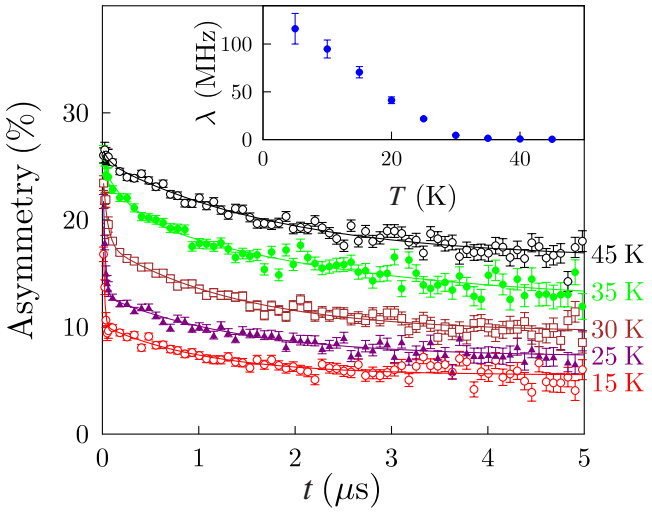

FIG. 5. (Color online) Muon-spin relaxation data for $FeMo_4Ge_3$ (sample A) at selected temperatures. The data are fitted with a relaxation function consisting of two exponentials, one with a large relaxation rate (dominant at short times) and one with a slow relaxation rate (dominant at long times). The inset shows the measured temperature dependence of the fast relaxation rate.

$=0.14$ J mol^{-1} K^{-2}, close to our fitted value. However, a close inspection of the match between the observed and modeled heat capacities reveals that the data are not well accounted for below 30 K. The temperature dependence of the residual heat capacity, assumed to be magnetic in origin, is shown in the inset of Fig. 4. The residual shows a broad maximum between 15 and 23 K, and a weak feature at 7 K. The small size of these features suggests that the entropy change associated with these transitions is very small. The heat capacity of sample B above 30 K was equally well fitted by the same model [$\Theta_D=370(8)$ K, $\Theta_E=161(3)$ K, and $\gamma=0.186$ J mol^{-1} K^{-2}] but again a residual heat capacity, shown in the inset of Fig. 4, was observed at low temperature. In this case, a sharper maximum is present at a lower temperature (12 K), although the feature at 7 K is still observed. The form of the heat capacity observed in these two samples is quite similar to that observed in a number of canonical spin glasses. In $Au_{1-x}Fe_x$,[16] a small magnetic contribution with a broad peak around the spin-glass or freezing temperature is observed for $x<0.15$. For $x>0.15$, two peaks are observed, both broad, and relatively well separated. For both regimes, the residue has a very similar magnitude to that found in our data, although the characteristic temperatures are much higher.[16] Measurements on $Cu_{1-x}Mn_x$ also show a broad peak around the temperature where the cusp is observed in ac susceptibility measurements.[17] Studies on the intercalated transition-metal dichalcogenide Fe_xNbS_2 (Ref. 18) show that for $x=0.325$, sharply defined peaks in the heat capacity are observed, which is consistent with an antiferromagnetic ordering transition together with two unidentified anomalies; reducing the Fe concentration to $x=0.309$ left a broad peak in the excess heat capacity, with three anomalies evident around the top of the peak, although their origin was not identified. This behavior is very similar to our own data, having similar magnitude, but occurring at a higher temperature. At lower iron concentrations, apart from $x=0.239$, which orders antiferromagnetically, the excess heat capacity was further reduced, although small steps were evident, coincident with spin-glass-like transitions reported in magnetic susceptibility measurements.

Figure 5 shows muon-spin relaxation data from sample A measured at five temperatures. We note first the absence of oscillations in the muon asymmetry at all measured temperatures; the spectra are purely relaxing across the entire measured temperature regime. Oscillations are expected in the muon spectra for a material showing commensurate long-range magnetic order, and also for some incommensurate long-range-ordered spin structures. The absence of these oscillations points to a broad distribution of magnetic fields at the muon sites in sample A. We also note that there is no missing fraction of asymmetry, which might imply the existence of long-range order: the initial asymmetry (measured at $t=0$) corresponds to $\sim 25\%$, the theoretical maximum expected for the geometry of detectors in the sample.

Above 30 K, the spectra are well described by a simple exponential relaxation $\exp(-\Lambda t)$. As the sample is cooled, the asymmetry is relaxed by a sum of two relaxation functions in the form

$$A(t) = A_1 f(\lambda t) + A_2 \exp(-\Lambda t), \tag{1}$$

where $f(\lambda t)$ is a rapidly decaying function of time.

The observed temperature behavior of our data is reminiscent of the case of a canonical spin glass,[19] although, as we shall show, a detailed analysis shows several differences. In the case of a dilute alloy spin glass at low temperatures, the coexistence of static and dynamic local fields at the muon site gives rise to a relaxation of the two-component form given in Eq. (1). The first component, with amplitude A_1, describes the evolution of the muon-spin components perpendicular to the local magnetic field direction at the muon sites (expected to be $2/3$ of the total amplitude), which are relaxed by both static and dynamic local fields. The second component, with amplitude A_2 (expected to account for the remaining $1/3$ of the polarization), describes the muon-spin components parallel to the local magnetic fields, relaxed purely by dynamic fluctuations.

For the dilute alloy, the dynamic relaxation results in "root exponential" relaxation of the form $\exp[-(\Lambda t)^{1/2}]$, which we do not observe. The root exponential arises from fluctuations of the local magnetic field of muons, where the local fields are drawn from a distribution of field distributions,[19] each with its own second moment $\Delta^2 = \gamma_\mu^2 \langle (B-\langle B \rangle)^2 \rangle$ (where γ_μ is the muon gyromagnetic ratio), reflecting the range of possible muon positions with respect to the dilute magnetic ions. In contrast, the observed simple exponential (with amplitude A_2) results from the dynamic fluctuations of muon sites all drawing from the same distribution of local magnetic fields (i.e., from a distribution described by a single Δ).[20] This is attributable to the fact that the Fe atoms in sample A are not dilute, so the field distribution will be better described by a single field width Δ.

Despite this, our results may be explained with a similar argument to the conventional spin-glass case. In general, static magnetism with, or without, long-range order results in

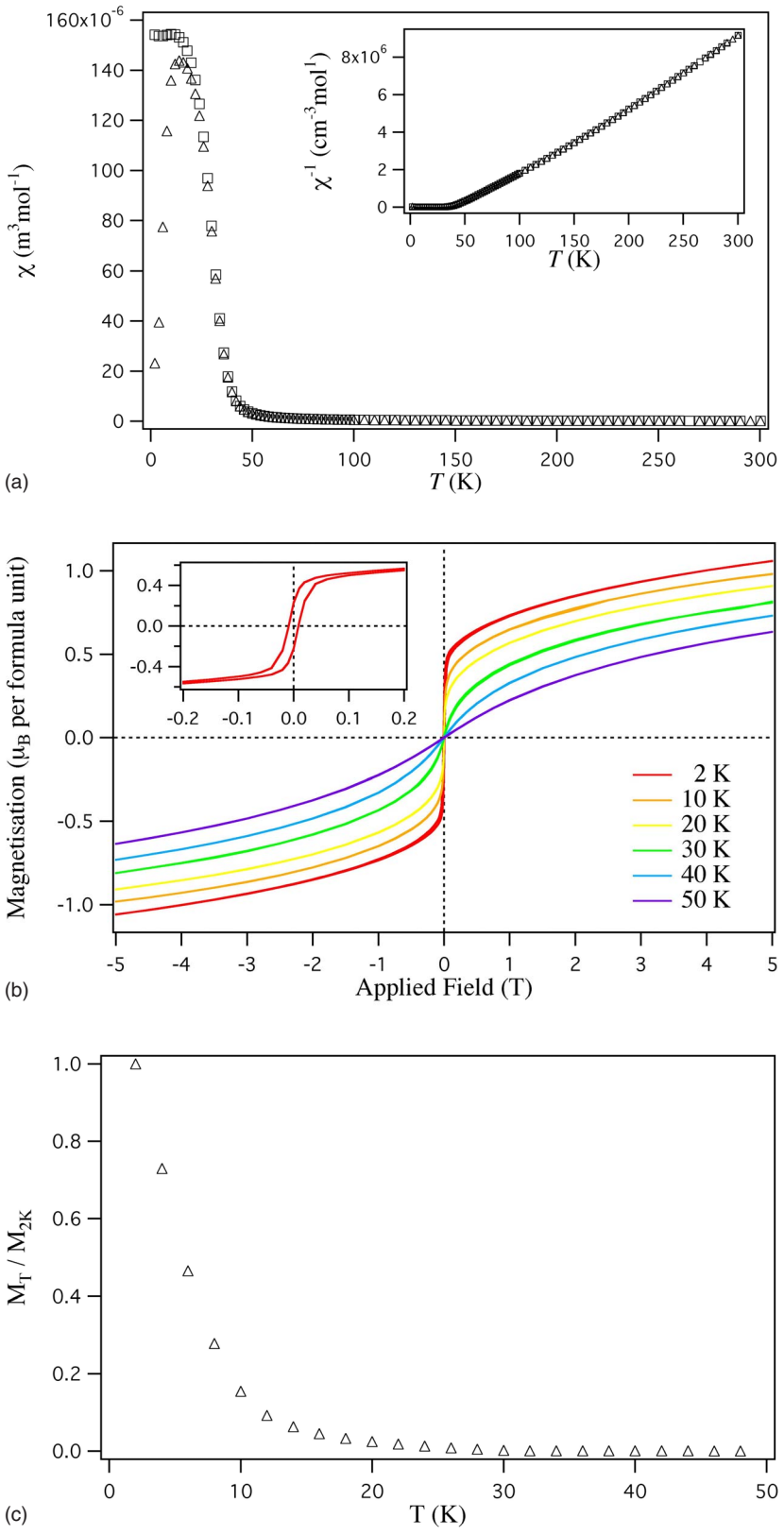

FIG. 6. (Color online) (a) Molar dc magnetic susceptibility of $FeMo_4Ge_3$ (sample A) as a function of temperature and (b) magnetization as a function of applied field at temperatures below 50 K. In the upper-right quadrant, the measuring temperature increases from 2 to 50 K on descending from the uppermost curve to the lowest. The sequence is reversed in the lower-left quadrant. The inset is an enlargement of the data collected at 2 K. (c) Thermal-remanent magnetization (normalized to the value at 2 K) as a function of temperature.

a rapid initial muon relaxation due to the corresponding distribution of static local fields at the muon sites. The appearance, below around ~25 K, of the fast relaxing component with amplitude A_1, which coexists with the slowly relaxing simple exponential (with amplitude A_2), points toward the coexistence of broad distributions of both static spin disorder and spin fluctuations at low temperatures. As the temperature is increased, the dynamics gradually dominate the muon response until, above ~25 K, the spin relaxation is entirely dynamic and is described by a single exponential. This behavior is again similar to that of the canonical spin glass, where the mixed static and dynamic components may be-

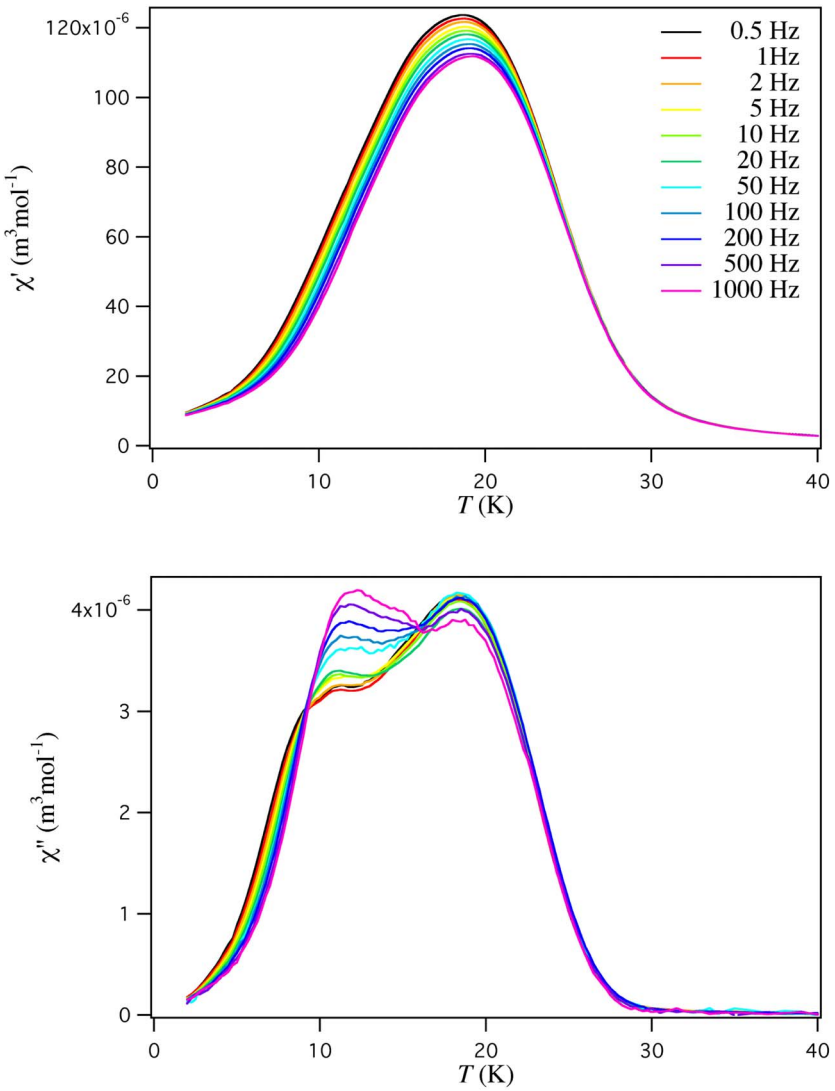

FIG. 7. (Color online) Molar ac susceptibility of $FeMo_4Ge_3$ (sample A) in zero dc field as a function of temperature and frequency. In the case of χ' the frequency increases from 0.5 to 1000 Hz on descending from the uppermost curve to the lowest. The same sequence is observed in χ'' below the crossover point at ~10 K.

come purely dynamic as the temperature is increased through the spin freezing transition.[19]

For our data, the large magnitude of the relaxation rate λ at low temperatures where $\lambda \sim 100$ MHz, makes it difficult to assign the function $f(\lambda t)$ a particular form. Static relaxation, drawn from a single Gaussian distribution of magnetic fields with second moment Δ, should result in the Kubo–Toyabe relaxation function[20] (which is approximately Gaussian at early times). We note also that the distribution of disordered static local fields in a spin glass is often Lorentzian[19] and leads to exponential relaxation. Whatever the case here, it is highly likely that the mixed static and dynamic forms of the magnetic behavior suggested above would cause this function to be more complicated as is in the dilute spin-glass case.[19] In our analysis, we have used a simple exponential in order to extract the general behavior of the relaxation rate. In our fitting routine, the small relaxation rate Δ remained fixed at $\Delta = 0.2$ MHz and the fast relaxation rate λ was allowed to vary across the measured temperature regime. The resulting behavior of λ is shown in the inset of Fig. 5, where we see that λ increases with cooling, reflecting the freezing of spins below $T \sim 25$ K. Following the approach of Uemura *et al.*,[19] we may roughly estimate the relaxation rate expected in analogy to the dilute spin-glass case. Typically, the dipole fields for a lattice of Fe atoms will give a second moment at a muon site of $\Delta_{max} \sim 1$ GHz. By taking the lattice concentration of Fe atoms in sample A to be ~10%, we estimate that $\lambda \sim 0.1\Delta_{max}$, giving the order of magnitude that we observed at the lowest temperatures.

A more detailed analysis might be possible by using results of longitudinal field decoupling experiments (not performed to date), but we would not expect these to alter the main conclusions that we can draw from the data, e.g., that our μ^+SR results point toward some degree of spin freezing, giving rise to a broad distribution of static disorder coexisting with dynamic fluctuations below a temperature of ~25 K and to purely dynamic fluctuations above this temperature.

The temperature dependence of the dc molar magnetic susceptibility (defined as M/H) of sample A is shown in Fig. 6(a). Fitting the data in the range $150\ \text{K} \leqslant T \leqslant 300$ K to a Curie–Weiss law resulted in an effective magnetic moment $\mu_{\text{eff}} = 4.57(1)\mu_B$ per Fe atom and a Weiss constant $\theta = 49.8(7)$ K. Below 50 K, the susceptibility rises, with the gradient $d\chi/dT$ being steepest at 30 K. The FC susceptibility is constant below 14 K, the temperature at which χ_{ZFC} reaches a maximum. The magnetization, shown in Fig. 6(b),

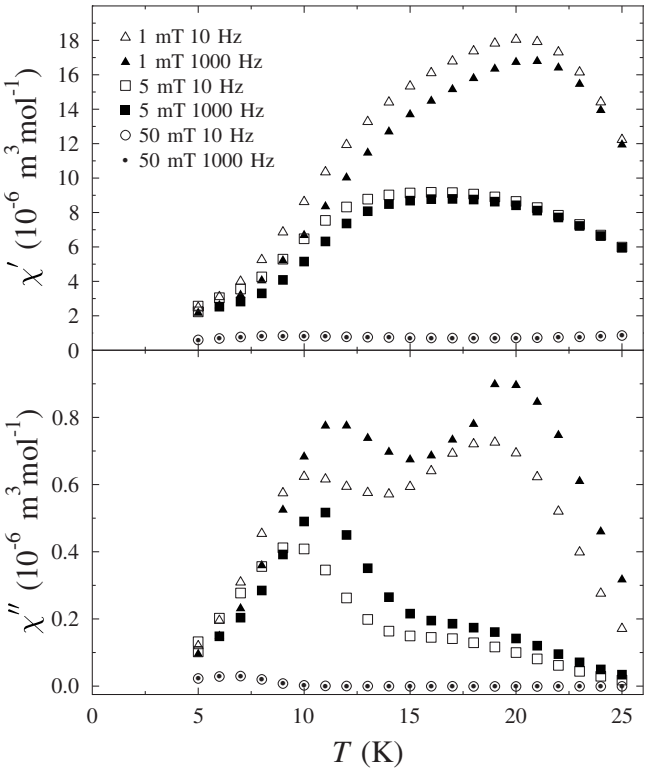

FIG. 8. Molar ac susceptibility of $FeMo_4Ge_3$ (sample A) as a function of temperature in different applied dc fields. The frequency of the ac excitation is also shown.

rapidly increases with applied field, reaching $\sim 0.5 \mu_B$/f.u. in a field of 0.1 T, but it does not saturate in a field of 5 T. The inset on Fig. 6(b) shows a remanent magnetization of $0.23(1) \mu_B$/f.u. and a coercive field of 8.7(1) mT at 2 K. No demagnetizing factor has been applied to any of our magnetic data. The thermal-remanent magnetization [Fig. 6(c)] decreased on warming from 2 K and was effectively zero at 30 K.

The temperature and frequency dependence of the ac susceptibility of sample A is unusual (Fig. 7). The real part, χ', starts to rise at $\sim$35 K and reaches a maximum at a frequency-dependent temperature (T_f) close to 19 K. The imaginary component, χ'', rises below $\sim$28 K and also reaches a local maximum at a frequency-dependent temperature close to 19 K. However, whereas χ' smoothly decreases on further cooling, χ'' rises to a second local maximum at $\sim$12 K, with the exact temperature having a different frequency dependence from that observed at about 19 K. The temperatures derived by curve fitting for the three maxima at a frequency of 1 kHz are T_f=19.17(1), $T_1(\chi''_{max})$=18.45(6), and $T_2(\chi''_{max})$=12.09(4) K, and at 10 Hz, T_f=18.81(1), $T_1(\chi''_{max})$=18.43(1), and $T_2(\chi''_{max})$=11.28(7) K. The ac susceptibility shows a strong dependence on the strength of the applied dc field, as can be seen by a comparison of Figs. 7 and 8. In a dc field of 1 mT, the data are qualitatively very similar to the results obtained when the dc magnetic field in the SQUID magnetometer was adjusted to zero, showing two peaks in χ'' at $\sim$19 K and 11 K. However, the frequency dependence of $T_1(\chi''_{max})$ markedly increases when a field is applied. In a dc field of 5 mT, both peaks are reduced, although the transition at 19 K is more strongly suppressed. With a dc field of 50 mT, the susceptibility is reduced over the whole temperature range. The temperature (T_f) of the maximum in the real component of the susceptibility was determined using a curve fitting procedure. The scaling parameter,[9] $\Delta T_f/[T_f \Delta(\log \omega)]$, that characterizes the frequency (ω) dependence of T_f takes a value of 0.01 for sample A of $FeMo_4Ge_3$.

The temperature dependence of the dc molar magnetic susceptibility of sample B is shown in Fig. 9(a). It is clearly different from that of sample A. The gradient $d\chi/dT$ is steepest at 16 K and both the ZFC and FC data show a maximum at 12 K. Furthermore, the magnitude of χ_{max} is only $\sim$30% of that of sample A. The FC susceptibility is constant below 5 K, whereas the ZFC value decreases down to the lowest temperature measured. Similar to that of sample A, the magnetization of sample B at 2 K, shown in Fig. 9(b), does not saturate in a field of 5 T; the magnetization in this field is approximately 20% lower than that of sample A. Sample B gives a somewhat more open hysteresis loop with a coercive field of 35(1) mT and a remanent magnetization of 0.12(1) μ_B/f.u.

The ac susceptibility of sample B (Fig. 10) also differs from that of sample A. The real part of the susceptibility displays a frequency-dependent maximum at $\sim$13 K, and the imaginary component has a maximum at $\sim$11 K. No second maximum in χ'' is observed at lower temperatures, although the frequency crossover in χ'' observed at $\sim$9 K in sample A is also observed in sample B, albeit at a lower temperature ($\sim$7 K). The temperatures derived by curve fitting for the maxima at a frequency of 1 kHz are T_f=13.17(1) and $T_1(\chi''_{max})$=11.43(2) K, and at 10 Hz, T_f=12.89(2) and $T_1(\chi''_{max})$=10.97(2) K. The scaling parameter $\Delta T_f/[T_f \Delta(\log \omega)]$ takes a value of 0.01 for sample B of $FeMo_4Ge_3$, as it did for sample A.

The iron-57 Mössbauer spectra of sample A obtained at 85 and 295 K are shown in Fig. 11; the spectra obtained from sample B look very similar. At and above 85 K, both samples appear to be paramagnetic, which is in agreement with the magnetic measurements. It proved possible to fit the spectra of both samples with a model consisting of two symmetric quadrupole doublets having the same linewidth; the resulting parameters are given in Table II and their temperature dependence is illustrated in Fig. 12. On the basis of their relative areas, the two doublets have been assigned to a fourfold site and a 16-fold site. Both the isomer shift and quadrupole splitting of the fourfold site are larger than for the 16-fold site and the quadrupole splitting, and relative areas are essentially independent of temperature for both sites in both samples. We shall describe the Mössbauer spectra collected at 4.2 K only briefly because the quality of our data demonstrated that a detailed study of the low-temperature region will require the use of a sample enriched with iron-57. However, the spectrum of sample A obtained at 4.2 K clearly indicated that $\sim$90% of the iron on the fourfold site exhibits a static spin state with an average hyperfine field of $\sim$16 T; the linewidths of the magnetic sextet were broad. In contrast, the iron on the 16-fold site is either paramagnetic or exhibits a weak hyperfine field of at most 1 T. The remaining hyperfine parameters were consistent with those measured at higher temperatures.

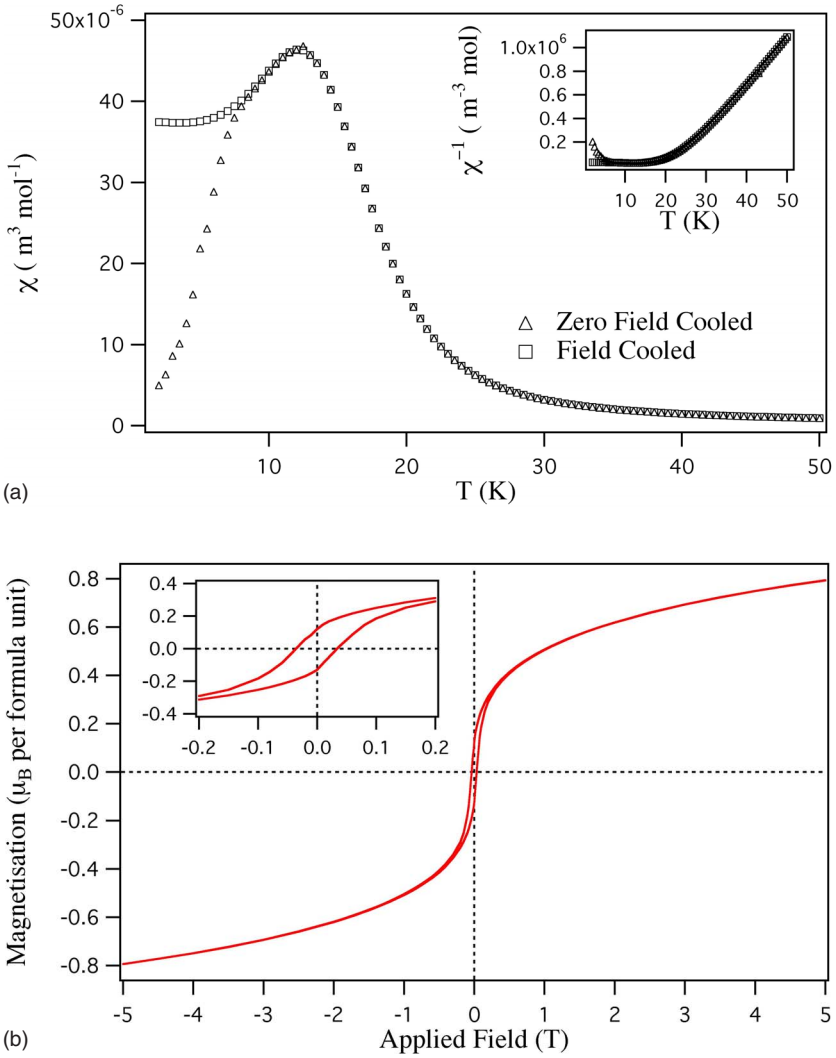

FIG. 9. (Color online) (a) Molar dc magnetic susceptibility of $FeMo_4Ge_3$ (sample B) as a function of temperature. (b) Magnetization as a function of applied field at 2 K.

The Mössbauer spectral data thus suggest that the local environment of the iron atoms is the same or very similar in samples A and B, despite the fact that the susceptibility and heat-capacity data reveal that the two samples show differing magnetic behavior. In order to rationalize this apparent inconsistency, it is necessary to identify a way to modify the three-dimensional crystal structure while retaining the local environment of the iron atoms. The structural analysis of sample B had revealed unit-cell parameters slightly, but significantly, different from those of sample A. Furthermore, the degree of iron/molybdenum ordering appeared to be different. The latter observation takes on a greater significance when considered in the light of the Mössbauer spectra, which show that the atomic distribution is essentially the same in both samples. In an attempt to resolve this, the x-ray data collected from sample B were reanalyzed using a number of different models, each with a different distribution of elements over the fourfold and 16*k* sites. A model in which iron and molybdenum occupy the 4*a* sites and the 16*k* sites, with the chain of germanium atoms moving to the 4*b* sites, gave a good account of the x-ray data (R_{wpr}=5.15%) and the iron:molybdenum ratio on the 4*a* site was refined to be 73(1):27(1), which is in good agreement with the value derived from the spectroscopic data. This was the only model to account for both the x-ray diffraction and the Mössbauer spectral data in a satisfactory manner. We thus conclude that the iron and molybdenum atoms in $FeMo_4Ge_3$ occupy the 16*k* site and either the 4*a* site (sample B) or the 4*b* site (sample A), with the germanium atoms occupying the other fourfold site. We assume that, whichever fourfold site they occupy, the immediate environments of the iron atoms in the Fe/Mo chains are similar enough to result in similar values for the Mössbauer parameters, whereas the differences in coordination geometry beyond the nearest-neighbor shell are large enough to cause differences in the magnetic behavior.

Having identified a way in which the two samples might differ structurally, we attempted to synthesize each in a deliberate fashion. Following several closely monitored repetitions of the synthesis, we established that samples of type-A form when the initial reaction takes place at 973 K; sample B was reproducibly formed when an offset on the furnace controller resulted in an initial temperature of 983 K. For all the samples prepared, with structural refinements based on a model having iron located on the 4*b* and 16*k* sites, the Fe:Mo ratio on the 4*b* site was never refined to a value significantly different from those (~72:28 and 59:41) reported above, as might have been expected if the difference between the different types of sample was attributable to a variation in the

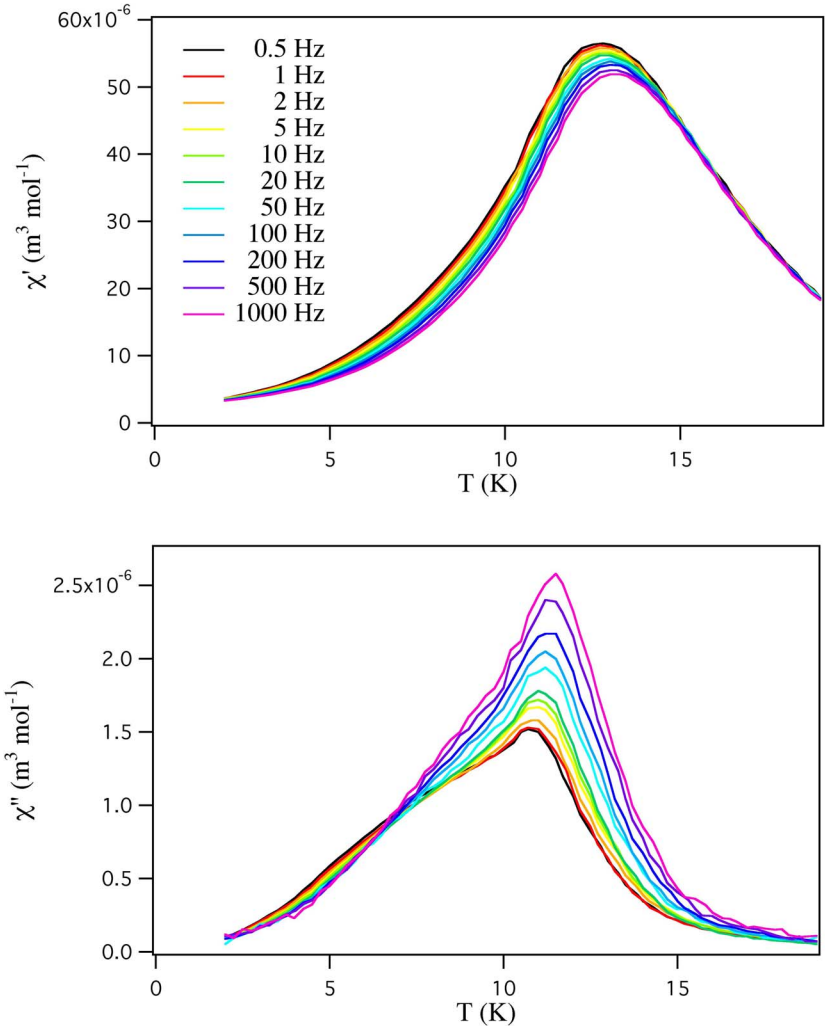

FIG. 10. (Color online) Molar ac susceptibility of $FeMo_4Ge_3$ (sample B) in zero dc field as a function of temperature and frequency. In the case of χ', the frequency increases from 0.5 to 1000 Hz on descending from the uppermost curve to the lowest. The inverse sequence is observed in χ''.

degree of atomic order within the same basic crystal structure. Furthermore, the unit-cell parameters never took values intermediate between those assigned above to samples A and B. The observation of these bimodal distributions lends support to our proposal that a more significant structural difference exists between sample types A and B. Once formed, samples of type B never transformed to type A, and vice versa. Hence, we deduce that the two forms of the structure have very similar energies and that kinetic factors prevent the transformation from one to the other.

DISCUSSION

The absence from the diffraction patterns of lines attributable to impurity phases demonstrates that the synthetic method described above can produce high-quality polycrys-

TABLE II. Mössbauer spectral hyperfine parameters for $FeMo_4Ge_3$. (The relative errors are given. The absolute errors are approximately twice as large.)

Sample	T (K)	δ[a] (mm s^{-1})	ΔE_Q (mm s^{-1})	Γ (mm s^{-1})	Area (%)	Assignment
A	295	−0.041(5)	0.45(1)	0.29(1)	29.7(5)	16-fold
		0.342(5)	0.61(1)	0.29(1)	70.3(5)	4-fold
	85	0.082(5)	0.49(1)	0.34(1)	26.7(5)	16-fold
		0.472(5)	0.61(1)	0.34(1)	73.3(5)	4-fold
B	295	−0.040(5)	0.45(1)	0.31(1)	30.8(5)	16-fold
		0.347(5)	0.62(1)	0.31(1)	69.2(5)	4-fold
	85	0.056(5)	0.46(1)	0.32(1)	31.4(5)	16-fold
		0.470(5)	0.62(1)	0.32(1)	68.6(5)	4-fold

[a]The isomer shifts are given relative to room-temperature α-iron foil.

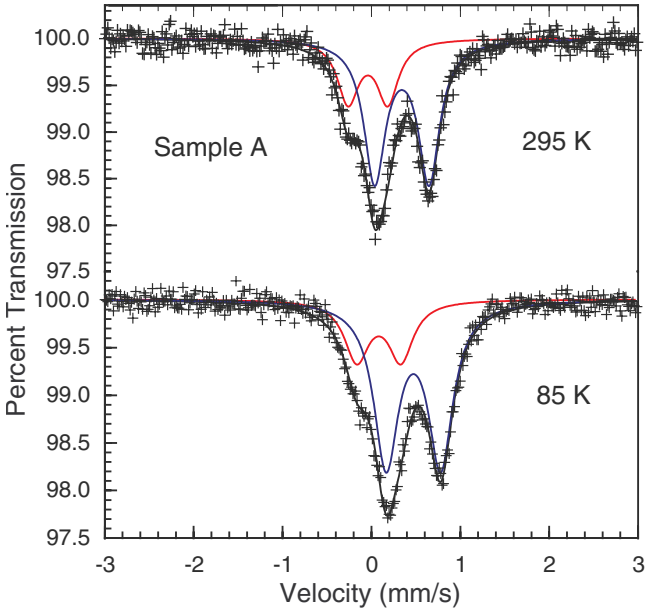

FIG. 11. (Color online) The iron-57 Mössbauer spectra of $FeMo_4Ge_3$ (sample A) obtained at 85 and 295 K.

talline samples of $FeMo_4Ge_3$. This is noteworthy in view of the contrast between the temperature used in our synthesis and those used previously to prepare related compositions. Ström *et al.*,[21] for example, used arc melting with subsequent annealing at 1873 K in order to prepare polycrystalline samples of compositions close to Mo_5Si_3. Our observation of atomic disorder over the 16-fold and fourfold sites in $FeMo_4Ge_3$ is consistent with their description of $CrMo_4Si_3$ and $TiMo_4Si_3$.

We discovered by sheer serendipity that a subtle change in our synthesis conditions can change the atomic distribution within the basic crystal structure and, consequently, cause a marked change in the properties of the reaction product. We shall discuss each form of the compound in turn.

The electronic properties of sample A are more complex. The transport data and the heat-capacity data are characteristic of a metallic material; we note that a two-parameter fit to the heat capacity of Mo_5Ge_3 in the temperature range $1.6\ \mathrm{K} < T < 10\ \mathrm{K}$ resulted[3] in the values $\theta_D = 377$ K and $\gamma = 0.012\ \mathrm{J\ mol^{-1}\ K^{-2}}$. The absence of magnetic Bragg scattering in the neutron diffraction data collected at 5 K and of oscillations in the time dependence of the μ^+SR asymmetry proves the absence of long-range magnetic order in A-type $FeMo_4Ge_3$. However, the value of the Weiss constant measured by dc magnetometry shows that ferromagnetic interactions exist within the structure, and the results of the μ^+SR, magnetometry, and heat-capacity experiments suggest that a sequence of magnetic transitions does occur on cooling below ~35 K. Taken in isolation, the sharp rise in the dc magnetic susceptibility could be explained in terms of the formation of a magnetic cluster glass. The failure of the atomic magnetization to saturate in a field of 5 T, the strong field and frequency dependence of the ac susceptibility, the temperature dependence of the thermal-remanent magnetization, and the preliminary low-temperature Mössbauer data are all consistent with such an interpretation. The value of the parameter $\Delta T_f/[T_f \Delta(\log \omega)]$ is larger than those reported for most metallic spin glasses [e.g., 0.005 in CuMn (Ref. 8)], but significantly smaller than those reported for insulating spin glasses [e.g., 0.05 in $Eu_xSr_{1-x}S$ (Ref. 7)], and the susceptibility data are thus consistent with the transport data in suggesting that this compound behaves as a metallic magnetic glass with a low carrier density.

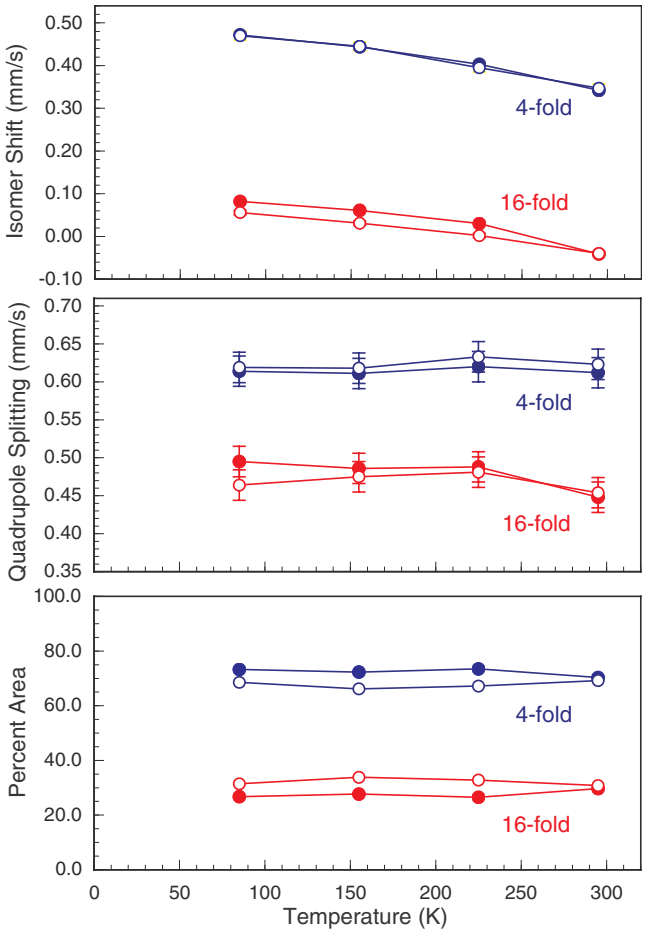

FIG. 12. (Color online) Temperature dependence of the iron-57 Mössbauer spectral parameters of sample A (filled circles) and sample B (hollow circles) of $FeMo_4Ge_3$. Unless shown, the error limits are no larger than the size of the data points.

However, the presence of two local maxima in χ'' shows that this interpretation would be an oversimplification. Furthermore, the broad maximum in the residual heat capacity, after the subtraction of the lattice and metallic components, is also indicative of a more complex magnetic behavior. It is not clear exactly what magnetic changes are represented by the maxima in the ac susceptibility and the heat capacity; further experimental work would be needed in order to clarify this issue. However, it is interesting to note that Motohashi *et al.*[22] observed a similar behavior in the ac susceptibility of the metallic, $n=2$ Ruddlesden–Popper phase Sr_3FeCoO_7. They postulated that the maximum in χ'' at the higher temperature corresponds to the formation of ferromagnetic clusters, and that the second maximum marks the freezing of the spin alignment of these clusters, thus forming a reentrant spin-glass phase. The temperature separation of the two transitions (at ~40 and 80 K) is somewhat greater in

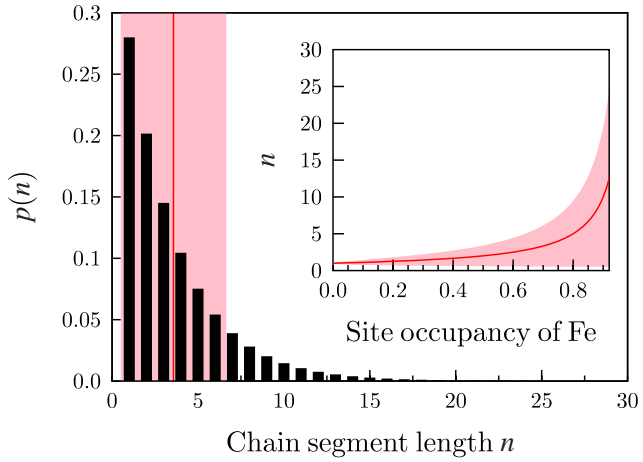

FIG. 13. (Color online) The probability $p(n)$ of a chain segment of n atoms of Fe is shown for the site occupancy of Fe equal to 0.72. The thin vertical line (red/black) shows the position of the mean of this probability distribution and the lightly shaded region (pink/gray) shows lengths within one standard deviation of the mean. The curve (red/black) in the inset shows the mean chain segment length $\langle n \rangle = 1/(1-q)$ and the shaded area (pink/gray) identifies the region within one standard deviation $[1 \pm \sqrt{q}]/(1-q)$ as a function of Fe site occupancy q.

the Ruddlesden–Popper phase than it is in our material, but it is possible that they have a common origin.

Whatever the details, the frequency dependence of the transition temperatures demonstrates that type-A $FeMo_4Ge_3$ behaves as some type of magnetic glass, and this glassy character is most likely to arise as a result of the disordered distribution of iron and molybdenum over the 4*b* and 16*k* sites. It is this disorder that defeats our original aim of studying the electronic properties of a one-dimensional chain of iron atoms. Indeed, the relatively high value of T_f demonstrates that $FeMo_4Ge_3$ cannot be treated as a one-dimensional compound. As a consequence of the disorder, it is necessary to consider (16*k*, 16*k*) and (4*b*, 16*k*) Fe-Fe interactions in addition to those between atoms in isolated chains of 4*b* sites. In a metallic system, the strength of the magnetic exchange interaction is a sensitive function of distance, and the presence in these chains of $(Fe)_n$ units of different lengths is likely to be an important source of disorder and, hence, to be at least partially responsible for the complexity of the electronic properties. Figure 13 shows the most likely number of successive iron atoms in a chain segment as a function of the iron concentration on the 4*b* site. For a fractional site occupancy by iron of 0.72, segments containing four iron atoms are most likely, with a significant number of segments having lengths of between one and seven iron atoms. We propose that the aperiodic breaks in the chains of magnetic atoms or the interchain coupling must lead to the presence of antiferromagnetic interactions that frustrate the formation of an ordered ground state. We also note that in relatively iron-rich AuFe alloys, the magnetic interactions become more short ranged because of the damping of the Ruderman–Kittel–Kasuya–Yosida interactions as a consequence of disorder.[23] The observation of some (~10%) unfrozen iron spins on the fourfold site in the Mössbauer spectrum of sample A at 4.2 K is consistent with the probability (Fig. 13) of finding some isolated iron atoms in the chains. A planned detailed study of the Mössbauer spectra of an iron-57 enriched sample of $FeMo_4Ge_3$ between 4.2 and 20 K should prove useful in delineating the spin-glass behavior.

Although it was type-A $FeMo_4Ge_3$ that was selected for the detailed study, our characterization of sample B using ac susceptibility methods is sufficient to conclude that this form of the material also behaves as a spin glass at low temperatures. Both the magnetic data and the heat-capacity data suggest that the transition temperature, although reduced, is better defined in this case; the data shown in Fig. 10 are more typical of a canonical spin glass than are those shown for sample A in Fig. 7. The arguments presented above to explain the behavior of sample A in terms of the length of chain segments carry over to sample B, which contains the same type of chains, albeit located in a different part of the unit cell. The average nearest-neighbor environment of an iron atom is the same in sample B as in sample A, although their subsequent coordination shells differ. (It is noteworthy that chains of edge-sharing Ge_5 tetrahedra occur in sample B.) The differences in the outer coordination shells presumably cause the differences in the behavior of the two samples, thus providing further evidence that the magnetic interactions within this structure cannot be considered as one dimensional. More specifically, we can speculate that the more complex behavior of sample A is derived from the existence of short Fe-Ge distances that are present in A, but not in B. Alternatively, the change in the Fe-Fe distance between atoms on the fourfold site and the 16*k* site might be the important factor in determining the magnetic properties of this itinerant electron system. In the absence of the Mössbauer spectral data, which demand a model with an ~72:28 Fe:Mo distribution on a fourfold site, the magnetic behavior of sample B could have been interpreted within the structural model of sample A, with the change in magnetic behavior being attributed to the reduced concentration of iron (~59%) on the fourfold site. This emphasizes the value of a multi-technique approach in the characterization of new materials.

We note that the heat-capacity data on both samples show a feature at 7 K. We do not have an explanation for this.

In conclusion, we have shown that high-quality, monophasic samples of $FeMo_4Ge_3$ can be prepared. This compound adopts the W_5Si_3 structure and would ideally contain isolated chains of Fe atoms. However, partial disorder on the Fe and Mo sites results in a length distribution among the chain segments containing only Fe atoms. There are two possibilities for the crystallographic location of these chains, with the synthesis conditions determining which is selected. Type-A $FeMo_4Ge_3$ is a bad metal with a low carrier density and exhibits a small negative magnetoresistance. Despite the presence of ferromagnetic interactions, type A shows no long-range magnetic order detectable by neutron diffraction or μ^+SR but, instead, shows a glassy behavior that can be ascribed to the aperiodic breaks in the chains of magnetic atoms or to the interchain coupling. However, the glassy behavior observed is very different from that seen in the canonical spin glasses, which contain a much lower concentration of magnetic species. Type-B $FeMo_4Ge_3$ has been studied

in less detail, but also appears to behave as a spin glass, albeit in a more conventional and, therefore, less intriguing manner.

ACKNOWLEDGMENTS

We are grateful to EPSRC (GR/R88601) and ILL for the provision of neutron beam time. Part of this work was carried out at the Swiss Muon Source, Paul Scherrer Institute, Villigen, Switzerland, where Alex Amato gave technical assistance. We also acknowledge experimental assistance from Heather Lewtas and Dan Woodbridge (both of Oxford University) and Francis Pratt (of ISIS). F.G. acknowledges the financial support of the Fonds National de la Recherche Scientifique, Belgium, through Grants Nos. 9.456595 and 1.5.064.05.

*Author to whom correspondence should be addressed.
†peter.battle@chem.ox.ac.uk
‡s.blundell1@physics.ox.ac.uk

[1] B. Aronsson, Acta Chem. Scand. (1947-1973) **9**, 1107 (1955).
[2] R. Dronskowski and A. Simon, Z. Kristallogr. **197**, 131 (1991).
[3] A. K. Ghosh and R. Caton, Solid State Commun. **44**, 1083 (1982).
[4] A. K. Ghosh and D. H. Douglass, J. Low Temp. Phys. **27**, 487 (1977).
[5] W. G. Jung and O. J. Kleppa, J. Less-Common Met. **169**, 93 (1991).
[6] A. V. Tkachuk and A. Mar, J. Solid State Chem. **177**, 4136 (2004).
[7] H. Maletta and W. Felsch, Phys. Rev. B **20**, 1245 (1979).
[8] C. A. M. Mulder, A. J. vanDuyneveldt, and J. A. Mydosh, Phys. Rev. B **23**, 1384 (1981).
[9] J. A. Mydosh, *Spin Glasses* (Taylor & Francis, London, 1993).
[10] Y. Muro, S. Giri, G. Motoyama, H. Nakamura, and T. Kohara, J. Phys. Soc. Jpn. **74**, 1135 (2005).
[11] H. Nakamura, S. Giri, and T. Kohara, J. Phys. Soc. Jpn. **73**, 2971 (2004).
[12] H. M. Rietveld, J. Appl. Crystallogr. **2**, 65 (1969).
[13] A. C. Larson and R. B. von Dreele, General Structural Analysis System (GSAS), Los Alamos National Laboratories Report No. LA-UR 86-748, 1994 (unpublished).
[14] S. J. Blundell, Contemp. Phys. **40**, 175 (1999).
[15] J. S. Hwang, K. J. Lin, and C. Tien, Rev. Sci. Instrum. **68**, 94 (1997).
[16] K. A. Mirza and J. W. Loram, J. Phys. F: Met. Phys. **15**, 439 (1985).
[17] L. E. Wenger and P. H. Keesom, Phys. Rev. B **13**, 4053 (1976).
[18] Y. Yamamura, S. Moriyama, T. Tsuji, Y. Iwasa, M. Koyano, S. Katayama, and M. Ito, J. Alloys Compd. **383**, 338 (2004).
[19] Y. J. Uemura, T. Yamazaki, D. R. Harshman, M. Senba, and E. J. Ansaldo, Phys. Rev. B **31**, 546 (1985).
[20] R. S. Hayano, Y. J. Uemura, J. Imazato, N. Nishida, T. Yamazaki, and R. Kubo, Phys. Rev. B **20**, 850 (1979).
[21] E. Ström, S. Eriksson, H. Rundlöf, and J. Zhang, Acta Mater. **53**, 357 (2005).
[22] T. Motohashi, B. Raveau, M. Hervieu, A. Maignan, V. Pralong, N. Nguyen, and V. Caignaert, J. Phys.: Condens. Matter **18**, 2157 (2006).
[23] S. Khmelevskyi, J. Kudrnovsky, B. L. Gyorffy, P. Mohn, V. Drchal, and P. Weinberger, Phys. Rev. B **70**, 224432 (2004).